Stochastic gravitational-wave background from stellar core-collapse events

Bella Finkel
Skidmore College, Saratoga Springs, New York 12866, USA

Haakon Andresen
The Oskar Klein Centre, Department of Astronomy, AlbaNova, SE-106 91 Stockholm, Sweden

Vuk Mandic
School of Physics and Astronomy, University of Minnesota, Minneapolis, Minnesota 55455, USA

(Received 5 October 2021; accepted 7 March 2022; published 28 March 2022)

We estimate the stochastic gravitational-wave background arising from all stellar core-collapse events in the universe based on the gravitational-wave signal predictions of recent numerical simulations. We focus on waveforms from slowly or nonrotating stars and include rapidly rotating, highly massive progenitors as extreme case limits. Our most realistic estimates are more than one hundred times below the sensitivity of third-generation terrestrial gravitational-wave detectors and likely weaker than cosmological contributions to the stochastic gravitational-wave background.

DOI: 10.1103/PhysRevD.105.063022

I. INTRODUCTION

The stochastic gravitational-wave background (SGWB) arises from the superposition of gravitational-waves (GWs) from a variety of independent cosmological [1–23] and astrophysical sources [24–34]. We focus on the SGWB due to stellar core-collapse events [30–33]. At the end of their lifetime, stars larger than about 8 $M_\odot$ form a gravitationally unstable iron core which collapses until its inner layer overshoots nuclear density and a proto-neutron star (PNS) is formed. The still collapsing outer core "bounces" off the inner region and launches an outwards propagating shock wave. The shock loses energy as it passes through the core and eventually stalls. In most cases, shock revival is thought to be powered by the absorption of a fraction of the neutrinos emitted from the PNS by material behind the shock, which causes the shock to break out the stellar surface and reveals the explosion as an electromagnetic transient.

In a normal, nonrotating supernova most of the GW emission is expected to come from oscillations of the PNS, but other hydrodynamic processes can contribute a large fraction of the emission. Low-frequency emission (below 300 Hz) mainly comes from the standing accretion shock instability (SASI), a hydrodynamic instability in the gain region that drives large scale spiral and sloshing oscillations of the shock and is expected to arise in a fraction of core-collapses [35]. High-frequency emission (above 300 Hz) largely arises from oscillations of the PNS.

The nondetection of GW transients associated with core-collapse events has constrained the GW energy produced by core-collapse supernovae (CCSNe) and ruled out regions of the parameter spaces of extreme emission models [36,37]. However, these constraints on GW emission remain a few orders of magnitude higher than the predictions of multidimensional numerical simulations. Additionally, the first three observing runs of Advanced LIGO and Advanced Virgo and the first two data releases by the International Pulsar Timing Array have provided upper limit estimates for the isotropic SGWB [38–40].

Previous studies [30,32,41] computed the SGWB due to CCSNe using, predominantly, two-dimensional simulations. Two-dimensional simulations are unable to capture the effects of nonaxisymmetric instabilities and tend to systematically overestimate GW amplitudes [42]. We sample a variety of theoretical predictions of the GW signal from three-dimensional numerical core-collapse simulations with sophisticated hydrodynamics and neutrino transport treatments, of duration from hundreds of milliseconds to upwards of a second. We begin by reviewing the procedure for estimating the background of astrophysical sources. Next, we give an overview of the details of the numerical simulations and their GW signals. Finally, we discuss features of the background and its detectability by third-generation GW detectors, such as Cosmic Explorer (CE) [43].

II. CALCULATION OF THE SGWB FROM CCSNE

The stochastic gravitational-wave background is usually described by its dimensionless energy spectrum:

$$\Omega_{\mathrm{GW}}(f) = \frac{1}{\rho_c}\frac{\mathrm{d}\rho_{\mathrm{GW}}}{\mathrm{d}\ln f}, \tag{1}$$

where $\rho_{\rm GW}$ is the GW energy density in the frequency band $(f, f+df)$ and ρ_c is the critical energy density which gives a flat universe, $\rho_c = \frac{3H_0^2c^2}{8\pi G}$. Here, c is the speed of light, G is Newton's gravitational constant, and H_0 is the Hubble constant (= 67.7 km/s/Mpc [38]).

The normalized GW energy density $\Omega_{\rm GW}$ can be expressed in terms of the energy spectrum emitted by a single CCSN, $\frac{dE_{\rm GW}}{df_e}(f_e)$, by the equation

$$\Omega_{\rm GW}(f) = \frac{f}{\rho_c H_0}\int_0^{z_{\rm max}} dz \frac{R(z)\frac{dE_{\rm GW}}{df_e}(f_e)}{(1+z)E(\Omega_m,\Omega_\Lambda,z)}, \quad (2)$$

where f_e is the frequency emitted at the source ($f_e = f(1+z)$). $R(z)$ is the rate of stellar core-collapse events per comoving volume as a function of redshift, assumed to follow the star formation rate (SFR) $R_*(z)$ as

$$R(z) = \lambda_{\rm CC} R_*(z), \quad (3)$$

where $\lambda_{\rm CC}$ is the mass fraction of stars which experience core collapse. We estimate $\lambda_{\rm CC}$ from the Salpeter initial mass function (IMF) $\phi(m) = Nm^{-2.35}$ with the normalization $\int_{0.1\ {\rm M}_\odot}^{\infty}\phi(m)m dm = 1$ and the assumption that all stars whose mass is greater than 8 $\rm M_\odot$ undergo collapse. ($\rm M_\odot$ denotes units of solar mass.) With these assumptions,

$$\lambda_{\rm CC} = \int_{8\ {\rm M}_\odot}^{\infty}\phi(m)dm \approx 0.007\ {\rm M}_\odot^{-1}. \quad (4)$$

While this $\lambda_{\rm CC}$ estimate is approximate, we do not expect its uncertainty to be larger than a factor of two, implying that the uncertainty in $\lambda_{\rm CC}$ will not make a qualitative difference in our results.

We choose the SFR model proposed by [44]. This model fits the parametrized form from Springel and Hernquist [45],

$$R_*(z) = \nu\frac{pe^{q(z-z_m)}}{p-q+qe^{p(z-z_m)}}, \quad (5)$$

to the galaxy SFR derived by [46] to obtain the parameter values $\nu = 0.178\ {\rm M}_\odot/{\rm yr/Mpc}^3$, $z_m = 2.00$, $p = 2.37$, and $q = 1.80$. This model is based on observations of the galaxy luminosity function at high redshift. Using the SFR given in Eq. (15) of [47] based on UV and IR data gives only marginally lower background estimates which do not differ from our results by more than 30%. As discussed below, variations in the spectra obtained from simulations constitute a significantly larger source of uncertainty than the particular SFR chosen.

Equation (2) includes a factor of $1+z$ to account for cosmic expansion and convert time from the source frame to the observation frame. The function

$$E(\Omega_m,\Omega_\Lambda,z) = \sqrt{\Omega_m(1+z)^3+\Omega_\Lambda} \quad (6)$$

expresses the comoving volume's dependence on redshift. Ω_m and Ω_Λ are the energy density in matter and in dark energy for a flat cosmological model, $\Omega_m = 0.311$ and $\Omega_\Lambda = 0.689$ [48]. Writing Eq. (2) in terms of the SFR in Eq. (3), we have

$$\Omega_{\rm GW}(f) = \frac{8\pi G f\lambda_{\rm CC}}{3H_0^3c^2}\int dz \frac{R_*(z)\frac{dE_{\rm GW}}{df_e}(f_e)}{(1+z)E(\Omega_m,\Omega_\Lambda,z)}. \quad (7)$$

Note that Eq. (7). does not account for the delay time between the formation of a star and its core collapse. We have investigated the effect of this delay and found it to be negligible.

The spectral energy density of the GWs emitted by a core-collapse supernova is required to calculate its contribution to $\Omega_{\rm GW}$. The energy radiated as GWs to infinity by a source is given by [49]

$$E_{\rm GW} = \int_0^t d\tau\int T_{0\nu}n^\nu r^2 d\Omega, \quad (8)$$

where the angular integral should be performed over a spherical shell at infinity that encloses the source. The vector n^ν is a spacelike unit vector perpendicular to the surface of the spherical shell, r denotes the radial coordinate of a spherical coordinate system, t is the time duration of the signal, and $T_{\mu\nu}$ denotes the GW energy-momentum tensor which, in the transverse-traceless (TT) gauge, is given by

$$T_{\mu\nu} = \frac{c^5}{32\pi G}\langle(\partial_\mu h^{\rm TT}_{\gamma\lambda})(\partial_\nu h^{\gamma\lambda}_{\rm TT})\rangle, \quad (9)$$

here $\langle\ldots\rangle$ denotes averaging over several wavelengths. Using the symmetries of the energy-momentum tensor in the TT-gauge we obtain

$$E_{\rm GW} = \frac{c^3}{16\pi G}\int_0^t d\tau\int r^2\langle(\partial_t h^{\rm TT}_\times)^2+(\partial_t h^{\rm TT}_+)^2\rangle d\Omega \quad (10)$$

(see [49,50] for details).

By applying Parsevals theorem to Eq. (10) one can show that the spectral energy density of the GW emission is given by

$$\frac{dE_{\rm GW}}{df} = \frac{c^3}{16\pi G}(2\pi f)^2\int r^2\langle(\tilde{h}^{\rm TT}_\times)^2+(\tilde{h}^{\rm TT}_+)^2\rangle d\Omega, \quad (11)$$

where $\tilde{h}^{\rm TT}_\times$ and $\tilde{h}^{\rm TT}_+$ denote the Fourier transforms of the cross and plus polarization modes of the GWs in the TT gauge, respectively [50,51]. Note that Eq. (11) will be slightly modified for a discrete signal and will depend on

the exact normalization and implementation of the discrete Fourier transform used, see [51] for details.

The angular dependence of the GW signal is needed for Eq. (11), but most numerical simulations do not provide this data. It is customary to publish the GW signal emitted in a few selected directions, which means that we are required to approximate the angular integral based on the data available to us.

III. CORE-COLLAPSE SIMULATIONS

We have begun to see convergences in the predictions of CCSNe GW signals [42,50,52–63], but the details of GWs emitted by CCSNe are stochastic and exhibit a large degree of variation. To ensure that our results are robust and represent the variation inherent to supernova GWs, we include a large set of theoretical signal predictions from numerical simulations. We have selected waveforms produced by different groups, with different numerical codes, and with different input physics. We focus on supernovae from non- or slowly rotating progenitors, which should make up more than 90 percent of all CCSNe.

Table I summarizes details of the simulations we use to calculate the background. We denote the models of [58] by "Rad" followed by the mass of the progenitor, and those of [64] by "Shib" followed by their rotation rate. Otherwise, we name the models as they are presented in the original papers.

We choose simulations from [57,60] which model core collapse in two nonrotating 18 $M_\odot$ red supergiants (s18 and s18np), a rapidly rotating 39 $M_\odot$ Wolf-Rayet star (m39), and a nonrotating 20 $M_\odot$ Wolf-Rayet star (y20). Model s18 is seeded with density perturbations from convective oxygen burning in its oxygen shell to aid in its explosion. No such perturbations are included in the s18np simulation, which prevents shock revival and allows the development of significant SASI activity. Model m39 has an initial surface rotation velocity of 600 km s^{-1}. Its high mass and rapid rotation produce strong GW emission, particularly at the equator.

Powell, Müller, and Heger model two nonrotating Pop-III stars of masses 100 $M_\odot$ (z100) and 85 $M_\odot$ (z85) in the pulsational pair instability regime [63]. Model z85 undergoes shock revival and collapses to a black hole before the end of its simulation, whereas the simulation of model z100 is terminated before shock revival or black hole collapse. Both models demonstrate strong GW emission across the frequency range we examine.

Radice *et al.* [58] model the collapse of seven nonrotating progenitors with ZAMS masses of 9 $M_\odot$, 10 $M_\odot$, 11 $M_\odot$, 12 $M_\odot$, 13 $M_\odot$, 19 $M_\odot$, 25 $M_\odot$, and 60 $M_\odot$. For all of these simulations, PNS oscillations are the main GW source. The models emit low-frequency GWs caused by prompt convection, then develop neutrino-driven convection or, in the case of Rad25, the SASI. The shock revives

TABLE I. Simulations from which we calculate the SGWB. The high-density nuclear equations of state (EOS) include SFHo and SFHx [65] and that of Lattimer and Swesty [66] with bulk incompressibility of K = 220 MeV (LS220).

Model name	ZAMS mass, type	Numerical code	EOS	Notes	Reference
m39	39 $M_\odot$, Wolf-Rayet star	CoCoNut-FMT [67]	LS220	Rotating, Exploding	[60]
s18np	18 $M_\odot$, giant		LS220	SASI	
y20	20 $M_\odot$, Wolf-Rayet star		LS220	Exploding	[57]
s18	18 $M_\odot$, giant		LS220	Exploding	
z100	100 $M_\odot$		SFHx	SASI	[63]
z85	85 $M_\odot$		SFHx	Exploding, SASI	
Rad9	9 $M_\odot$	FORNAX [68]	SFHo	Exploding	[58]
Rad10	10 $M_\odot$		SFHo	Exploding	
Rad11	11 $M_\odot$		SFHo	Exploding	
Rad12	12 $M_\odot$		SFHo	Exploding	
Rad13	13 $M_\odot$		SFHo		
Rad19	19 $M_\odot$		SFHo	Exploding	
Rad25	25 $M_\odot$		SFHo	Exploding, SASI	
Rad60	60 $M_\odot$		SFHo	Exploding	
s9-FMD-H	9 $M_\odot$, giant	AENUS-ALCAR [69]	SFHo	Exploding	[62]
s20-FMD-H	20 $M_\odot$, giant		SFHo		
s15nr	15 $M_\odot$	PROMETHEUS-VERTEX [70]	LS220	SASI	[56]
s15r	15 $M_\odot$		LS220	SASI	
s15fr	15 $M_\odot$		LS220	Rotating, Exploding, SASI	
mesa20-pert	20 $M_\odot$, giant	FLASH [71]	SFHo	SASI	[55]
mesa20	20 $M_\odot$, giant		SFHo	SASI	
Shib0	70 $M_\odot$	[72]	LS220	SASI	[64]
Shib1	70 $M_\odot$		LS220	Rotating, low-$T/\|W\|$ instability	
Shib2	70 $M_\odot$		LS220	Rotating, low-$T/\|W\|$ instability	

in all models except Rad13. Apart from Rad9, all exploding models show asymmetric accretion onto the PNS at late times and significant continued emission at the termination of the simulation.

From Andresen *et al.* [62] we select the two models s9-FMD-H and s20-FMD-H. The 9 $M_\odot$ model, s9-FMD-H, exhibits a low accretion rate onto the PNS and primarily emits at frequencies above 300 Hz with some low-frequency GW emission. The 20 $M_\odot$ model, s20-FMD-H, develops hot-bubble convection and significant SASI activity. The SASI activity appears as GW emission at frequencies below 250 Hz.

Andresen *et al.* [56] investigate the effects of moderate rotation with three 15 $M_\odot$ progenitors: one nonrotating (s15nr), one with central angular velocity $\Omega_0 = 0.2$ rad s^{-1} (s15r), and one fast rotating (s15fr) with central angular velocity $\Omega_0 = 0.5$ rad s^{-1}. We include all three modes in our analysis. Model s15fr experiences strong spiral SASI activity in the postshock flow before explosion. The SASI spiral mode is strong in s15nr. SASI activity is significantly weaker in s15r than in the other models, and the postshock region is dominated by convection.

O'Connor and Couch simulate the collapse of a 20 $M_\odot$ zero-age main-sequence star [55]. We use the GW signal from their three-dimensional, standard resolution models mesa20 and mesa20_pert, the latter of which is seeded with velocity perturbations in the silicon and oxygen shells when the simulation is mapped to FLASH [71]. Both mesa20 and mesa20_pert demonstrate SASI activity. Neither of these models explodes.

We also consider the 70 $M_\odot$ progenitors simulated with central angular velocities of $\Omega_0 = 0$ rad s^{-1}, $\Omega_0 = 1$ rad s^{-1},

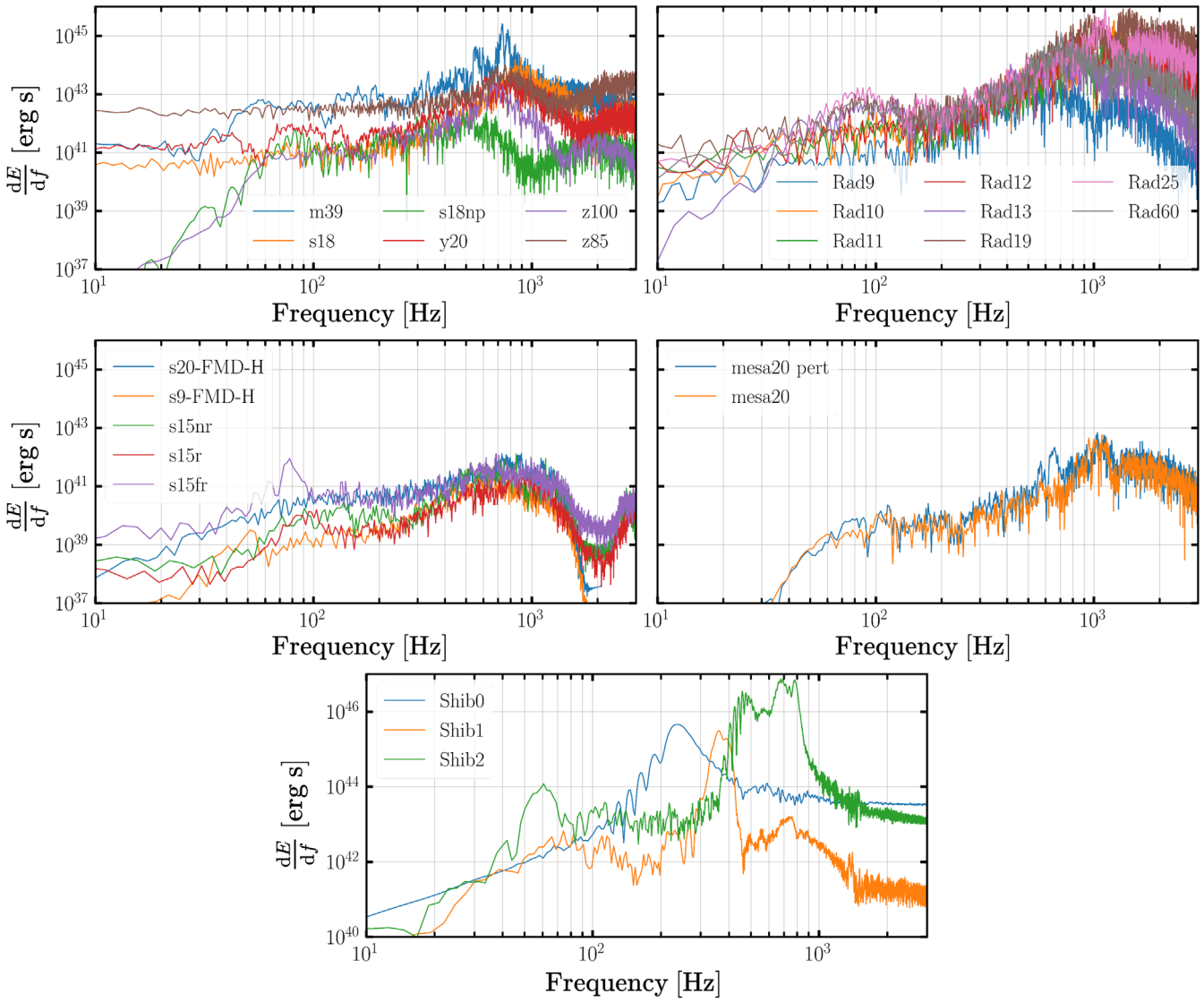

FIG. 1. Total time-integrated GW spectra $\frac{dE}{df}$ for emission from models by Powell and Müller [57,60,63] (upper left), Radice *et al.* [58] (upper right), Andresen *et al.* [56,62] (middle left), O'Connor and Couch [55] (middle right), and Shibagaki *et al.* [64] (bottom). The vertical axis range on the plot showing the models by Shibagaki *et al.* is higher than that for the other panels.

and $\Omega_0 = 2$ rad s^{-1} (Shib0, Shib1, and Shib2) by [64]. Before collapse, this star has a central iron core mass of $\sim$4.6 $M_\odot$. When the simulations are terminated, Shib0, Shib1, and Shib2 have PNS masses of $\sim$2.5 $M_\odot$, $\sim$2.2 $M_\odot$, and $\sim$2.6 $M_\odot$, respectively. The sloshing and spiral SASI modes of Shib0 produce strong GW emission between 200 and 300 Hz. The low-$T/|W|$ instability, where $T/|W|$ refers to the ratio of rotational and gravitational potential energy, is a rotational instability that can produce strong GW emission. It is observed in both rotating models, resulting in emission from 400 to 800 Hz in Shib2 and from 300 to 400 Hz in Shib1.

Fewer than ten percent of CCSNe are expected to arise from rapidly rotating progenitors [73]. Thus, it should be noted that the GW background spectra calculated below using models m39 and Shib2 represent the unrealistic scenario where all stars which undergo core collapse are rapidly rotating.

IV. RESULTS

We use the core-collapse GW energy spectra dE/df shown in Fig. 1 to calculate the normalized GW energy density $\Omega_{GW}(f)$. Our results are shown in Fig. 2. For each

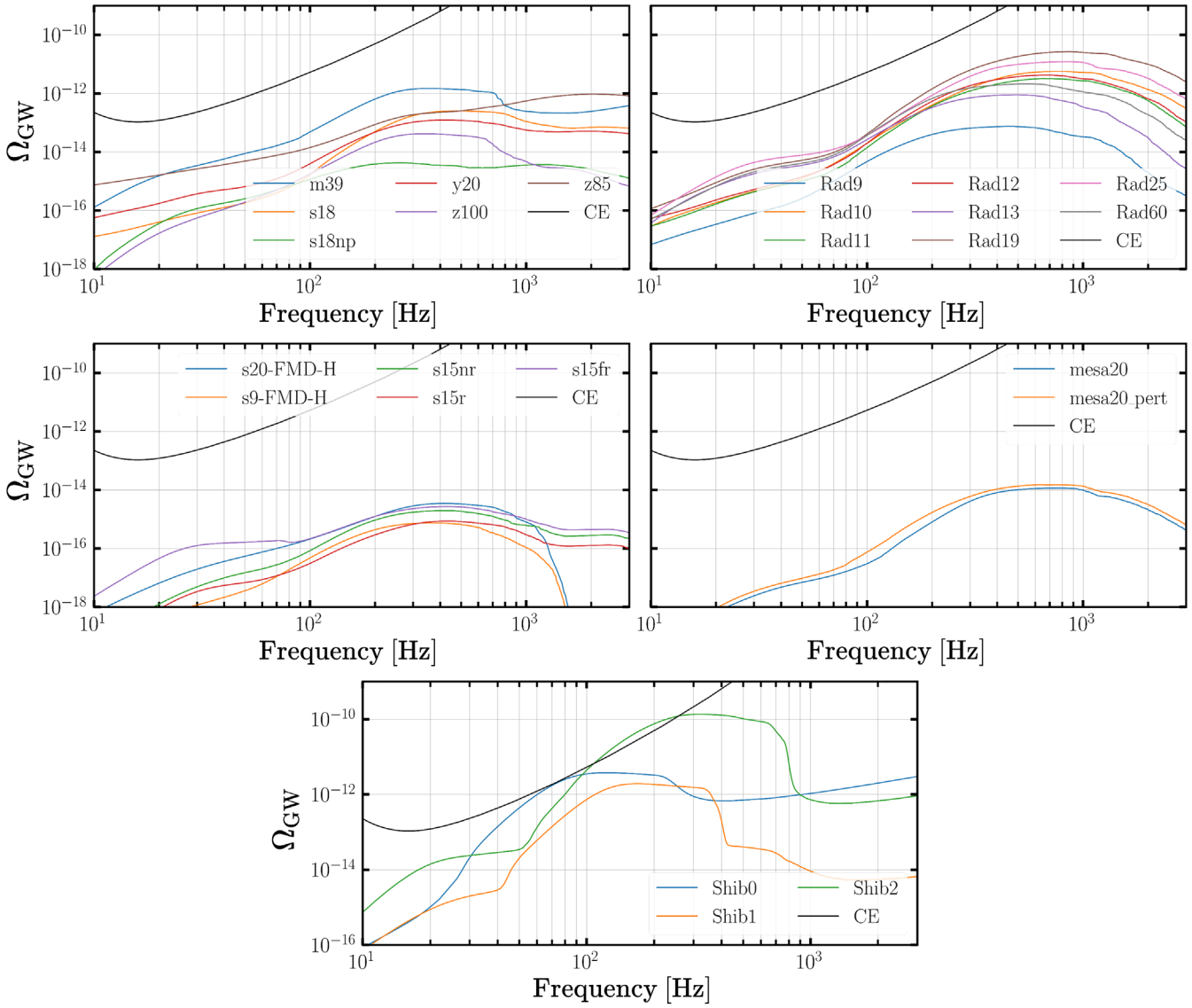

FIG. 2. Ω_{GW} for models by Powell and Müller [57,60,63] (upper left), Radice *et al.* [58] (upper right), Andresen *et al.* [56,62] (middle left), O'Connor and Couch [55] (middle right), and Shibagaki *et al.* [64] (bottom) shown in comparison with the 2σ power-law integrated sensitivity [77] of two collocated Cosmic Explorer [43] detectors assuming one year exposure. Note that these spectra are calculated under the assumption that all CCSNe events emit the same GW spectrum. In particular, the Shib1 and Shib2 models shown in the bottom panel are calculated under the unrealistic assumption that all CCSNe progenitors rotate rapidly and exhibit the low-$T/|W|$ instability.

curve in Fig. 2 we assume that all CCSNe have the same GW emission spectrum given by the corresponding core-collapse simulation model. As discussed above, the spectral properties of the signal are related to the physical properties of the supernova core (see [74–76] for further details).

All models yield backgrounds that would be undetectable by second-generation GW detectors, whose sensitivity is expected to reach $\Omega_{\rm GW}(f) \sim 10^{-9}$–$10^{-10}$. Most models yield backgrounds at least two orders of magnitude below the sensitivity of third-generation GW detectors, under the assumption of cross-correlating two collocated detectors of CE sensitivity [43] with one year of exposure.

The exceptions are the models by [64], which become borderline observable by CE, see the bottom panel of Fig. 2. However, this conclusion assumes that all CCSNe progenitors are rapidly rotating and develop the energetically-emitting low-$T/|W|$ instability. When these models are weighted by their prominence in the stellar population (about 1% of CCSNe are expected to arise from rapidly rotating progenitors [73]), their contribution to the overall SGWB becomes comparable to that of the other models. Considering only non- and slowly rotating models, Rad25 and Rad19 provide the strongest SGWB, and the model s15r yields the weakest SGWB.

We note that our results are subject to the uncertainty in the rate of CCSNe events across the universe, modeled in Eq. (7) by the star formation rate R_* and the scaling factor $\lambda_{\rm CC}$. While the scaling factor may be uncertain at the level of a factor of two, the star formation rate model is rather robust especially at redshifts smaller than two, which is where the majority of the CCSNe SGWB comes from.

We provide an averaged estimate of the background based on the relative abundances of nonrotating progenitors in Fig. 3. The contribution of each model to the background is weighted by its prominence in the stellar population as given by the normalized Salpeter IMF. We define the average spectrum

$$\Omega_A(f) = \frac{1}{\Gamma}\sum_i \phi(m_i)\Omega_i(f)\Delta m_i, \tag{12}$$

where $\Omega_i(f)$ is the background spectrum for the model(s) of mass m_i, and Δm_i extends from the halfway point between m_i and the model of the next lowest mass to the halfway point between m_i and the model of the next highest mass. In cases where there is more than one model of the same mass, we use a simple average between their background spectra for $\Omega(m_i)$. In Eq. (12), the normalization constant Γ is given by $\Gamma = \int_{8\ {\rm M}_\odot}^{100\ {\rm M}_\odot} \phi(m){\rm d}m$. It should be noted that the absence of a one-to-one relationship between the mass of the progenitor and the GW signal of its collapse, the stochastic nature of the signal, and the limited selection of core-collapse models mean that Fig. 3 is only of illustrative value, and should not be taken as a decisive estimate of the stochastic gravitational-wave background produced by core-collapse supernovae.

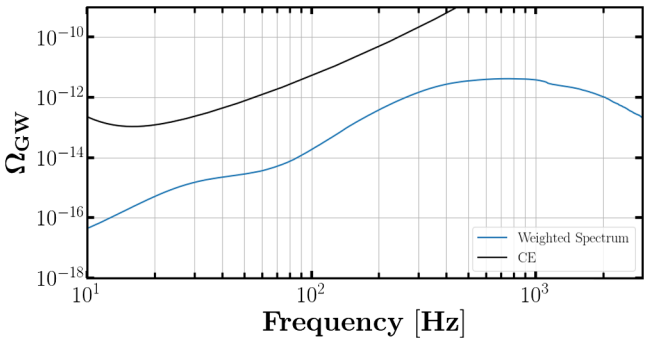

FIG. 3. Averaged $\Omega_{\rm GW}$ including the contributions of the nonrotating progenitors and excluding Shib0 weighted by the abundance of the stellar progenitor in the stellar population as given by the Salpeter IMF [cf. Eq. (12)].

V. CONCLUSIONS

In this work, we have estimated a range for the SGWB resulting from stellar core-collapse events using the results of three-dimensional numerical simulations of a variety of progenitors. The GWs emitted during core collapse are stochastic and associated with multiple emission processes. We find that in all but the most extreme cases, the SGWB from CCSNe is 2–5 orders of magnitude below the sensitivity of the third-generation GW detectors.

Our results are limited by the approximations used in the simulations we draw from and the characteristics of the stellar population we sample. All of the simulations shown in this paper were terminated at different times, in most cases while still emitting significant gravitational radiation. In extreme core-collapse scenarios appreciable GW emission occurs late in the explosion phase [78,79]. Longer simulations would provide a fuller assessment of the GW signal and a better picture of the background.

Anisotropic neutrino emission from the PNS can cause GW emission in the range of sub-Hertz to hundreds of Hertz [80–85]. A more complete description of the background would include the contribution of this signal, in particular at frequencies below the lower 10 Hz limit of our background calculations. Asymmetries resulting from the presence of magnetic fields can also lead to GW emission; magnetohydrodynamic effects have been found to significantly alter the GW signal [79,86].

At 10 Hz, the lower limit of the frequency range considered here, the core-collapse contribution to the SGWB is $\Omega_{\rm GW}(f) \sim 10^{-15}$ or weaker, meaning that cosmological GW backgrounds may be detectable over the core-collapse GW background. In many cases, the cosmological SGWB models are a few orders of magnitude stronger than our highest estimates for the CCSN background. For example, the backgrounds from cosmic string

networks in scaling with string tension $G\mu$ greater than 10^{-17} [3,5], primordial binary black hole coalescences involving masses greater than $10^{-6}\ M_\odot$ [87,88], and inflation mechanisms (e.g., those with an effective graviton mass between $m = 0$ H and $m = 0.9$ H, with a Hubble rate during inflation of $H = 10^{12}$ GeV or $H = 10^{13}$ GeV and tensor sound speed between $c_T = 0.2$ and $c_T = 1$, in natural units [89]) are expected to be one or more orders of magnitude above our predictions for the core-collapse background. These sources may therefore be accessible to future detectors, and their visibility will likely be unimpeded by the background due to CCSNe.

ACKNOWLEDGMENTS

V. M. would like to acknowledge the support of the NSF Grant No. PHY-2110238. B. F. would like to acknowledge the support of the NSF REU Grant No. 2049645. H. A. is supported by the Swedish Research Council (Project No. 2020-00452). The paper has been assigned designator LIGO-P2100353.

[1] T. Damour and A. Vilenkin, Gravitational radiation from cosmic (super)strings: Bursts, stochastic background, and observational windows, Phys. Rev. D **71**, 063510 (2005).
[2] X. Siemens, C. Creighton, I. Maor, S. Majumder, K. Cannon, and J. Read, Gravitational wave bursts from cosmic (super)strings: Quantitative analysis and constraints, Phys. Rev. D **73**, 105001 (2006).
[3] P. Auclair, J. J. Blanco-Pillado, D. G. Figueroa, A. C. Jenkins, M. Lewicki, M. Sakellariadou, S. Sanidas, L. Sousa, D. A. Steer, J. M. Wachter, S. Kuroyanagi, and LISA Cosmology Working Group, Probing the gravitational wave background from cosmic strings with LISA, J. Cosmol. Astropart. Phys. 04 (2020) 034.
[4] C. Ringeval and T. Suyama, Stochastic gravitational waves from cosmic string loops in scaling, J. Cosmol. Astropart. Phys. 12 (2017) 027.
[5] L. Sousa, P. P. Avelino, and G. S. F. Guedes, Full analytical approximation to the stochastic gravitational wave background generated by cosmic string networks, Phys. Rev. D **101**, 103508 (2020).
[6] J. J. Blanco-Pillado and K. D. Olum, Stochastic gravitational wave background from smoothed cosmic string loops, Phys. Rev. D **96**, 104046 (2017).
[7] R. Abbott *et al.* (LIGO Scientific Collaboration, Virgo Collaboration, and KAGRA Collaboration), Constraints on Cosmic Strings Using Data from the Third Advanced LIGO–Virgo Observing Run, Phys. Rev. Lett. **126**, 241102 (2021).
[8] L. Grishchuk, Amplification of gravitational waves in an istropic universe, J. Exp. Theor. Phys. **40**, 409 (1975).
[9] A. Starobinskii, Spectrum of relict gravitational radiation and the early state of the universe, JETP Lett. **30**, 682 (1979).
[10] M. Turner, Detectability of inflation-produced gravitational waves, Phys. Rev. D **55**, R435 (1997).
[11] R. Easther, J. T. Giblin, and E. A. Lim, Gravitational Wave Production at the End of Inflation, Phys. Rev. Lett. **99**, 221301 (2007).
[12] J. L. Cook and L. Sorbo, Particle production during inflation and gravitational waves detectable by ground-based interferometers, Phys. Rev. D **85**, 023534 (2012).
[13] C. J. Hogan, Gravitational radiation from cosmological phase transitions, Mon. Not. R. Astron. Soc. **218**, 629 (1986).
[14] E. Witten, Cosmic separation of phases, Phys. Rev. D **30**, 272 (1984).
[15] A. Kosowsky, M. S. Turner, and R. Watkins, Gravitational radiation from colliding vacuum bubbles, Phys. Rev. D **45**, 4514 (1992).
[16] A. Romero, K. Martinovic, T. A. Callister, H.-K. Guo, M. Martínez, M. Sakellariadou, F.-W. Yang, and Y. Zhao, Implications for First-Order Cosmological Phase Transitions from the Third LIGO-Virgo Observing Run, Phys. Rev. Lett. **126**, 151301 (2021).
[17] A. Lopez and K. Freese, First test of high frequency gravity waves from inflation using Advanced LIGO, J. Cosmol. Astropart. Phys. 01 (2015) 037.
[18] M. Geller, A. Hook, R. Sundrum, and Y. Tsai, Primordial Anisotropies in the Gravitational Wave Background from Cosmological Phase Transitions, Phys. Rev. Lett. **121**, 201303 (2018).
[19] C. Caprini, M. Hindmarsh, S. Huber, T. Konstandin, J. Kozaczuk, G. Nardini, J. M. No, A. Petiteau, P. Schwaller, G. Servant, and D. J. Weir, Science with the space-based interferometer eLISA. II: Gravitational waves from cosmological phase transitions, J. Cosmol. Astropart. Phys. 04 (2016) 001.
[20] A. Buonanno, M. Maggiore, and C. Ungarelli, Spectrum of relic gravitational waves in string cosmology, Phys. Rev. D **55**, 3330 (1997).
[21] M. Gasperini and G. Veneziano, The pre-big bang scenario in string cosmology, Phys. Rep. **373**, 1 (2003).
[22] V. Mandic and A. Buonanno, Accessibility of the pre-big-bang models to LIGO, Phys. Rev. D **73**, 063008 (2006).
[23] M. Gasperini, Observable gravitational waves in pre-big bang cosmology: An update, J. Cosmol. Astropart. Phys. 12 (2016) 010.
[24] B. P. Abbott *et al.* (LIGO Scientific and Virgo Collaborations), GW170817: Implications for the Stochastic Gravitational-Wave Background from Compact Binary Coalescences, Phys. Rev. Lett. **120**, 091101 (2018).
[25] B. P. Abbott *et al.* (LIGO Scientific and Virgo Collaborations), GW150914: Implications for the Stochastic

Gravitational Wave Background from Binary Black Holes, Phys. Rev. Lett. **116**, 131102 (2016).
[26] I. Cholis, On the gravitational wave background from black hole binaries after the first LIGO detections, J. Cosmol. Astropart. Phys. 06 (2017) 037.
[27] A. J. Farmer and E. S. Phinney, The gravitational wave background from cosmological compact binaries, Mon. Not. R. Astron. Soc. **346**, 1197 (2003).
[28] T. Regimbau and J. A. de Freitas Pacheco, Gravitational wave background from magnetars, Astron. Astrophys. **447**, 1 (2006).
[29] Q. Cheng, S.-N. Zhang, and X.-P. Zheng, Stochastic gravitational wave background from newly born massive magnetars: The role of a dense matter equation of state, Phys. Rev. D **95**, 083003 (2017).
[30] A. Buonanno, G. Sigl, G. G. Raffelt, H.-T. Janka, and E. Müller, Stochastic gravitational-wave background from cosmological supernovae, Phys. Rev. D **72**, 084001 (2005).
[31] S. Marassi, R. Schneider, and V. Ferrari, Gravitational wave backgrounds and the cosmic transition from Population III to Population II stars, Mon. Not. R. Astron. Soc. **398**, 293 (2009).
[32] K. Crocker, T. Prestegard, V. Mandic, T. Regimbau, K. Olive, and E. Vangioni, Systematic study of the stochastic gravitational-wave background due to stellar core collapse, Phys. Rev. D **95**, 063015 (2017).
[33] P. Sandick, K. A. Olive, F. Daigne, and E. Vangioni, Gravitational waves from the first stars, Phys. Rev. D **73**, 104024 (2006).
[34] V. Mandic, S. Bird, and I. Cholis, Stochastic Gravitational-Wave Background due to Primordial Binary Black Hole Mergers, Phys. Rev. Lett. **117**, 201102 (2016).
[35] J. M. Blondin, A. Mezzacappa, and C. DeMarino, Stability of standing accretion shocks, with an eye toward core-collapse supernovae, Astrophys. J. **584**, 971 (2003).
[36] B. Abbott, R. Abbott, T. Abbott, M. Abernathy, F. Acernese, K. Ackley, C. Adams, T. Adams, P. Addesso, R. Adhikari *et al.*, First targeted search for gravitational-wave bursts from core-collapse supernovae in data of first-generation laser interferometer detectors, Phys. Rev. D **94**, 102001 (2016).
[37] B. P. Abbott *et al.* (LIGO Scientific Collaboration and Virgo Collaboration), Optically targeted search for gravitational waves emitted by core-collapse supernovae during the first and second observing runs of advanced LIGO and Advanced Virgo, Phys. Rev. D **101**, 084002 (2020).
[38] R. Abbott *et al.* (The LIGO Scientific Collaboration and the Virgo Collaboration and the KAGRA Collaboration), Upper limits on the isotropic gravitational-wave background from advanced ligo's and advanced virgo's third observing run, Phys. Rev. D **104**, 022004 (2021).
[39] J. P. W. Verbiest *et al.*, The international pulsar timing array: First data release, Mon. Not. R. Astron. Soc. **458**, 1267 (2016).
[40] J. Antoniadis *et al.*, The International Pulsar Timing Array second data release: Search for an isotropic gravitational wave background, Mon. Not. R. Astron. Soc. **510**, 4873 (2022).
[41] D. M. Coward, R. R. Burman, and D. G. Blair, Simulating a stochastic background of gravitational waves from neutron star formation at cosmological distances, Mon. Not. R. Astron. Soc. **329**, 411 (2002).
[42] H. Andresen, B. Mller, E. Mller, and H.-T. Janka, Gravitational wave signals from 3D neutrino hydrodynamics simulations of core-collapse supernovae, Mon. Not. R. Astron. Soc. **468**, 2032 (2017).
[43] B. Abbott *et al.*, Exploring the sensitivity of next generation gravitational wave detectors, Classical Quantum Gravity **34**, 044001 (2017).
[44] E. Vangioni, K. A. Olive, T. Prestegard, J. Silk, P. Petitjean, and V. Mandic, The impact of star formation and gamma-ray burst rates at high redshift on cosmic chemical evolution and reionization, Mon. Not. R. Astron. Soc. **447**, 2575 (2015).
[45] L. Hernquist and V. Springel, An analytical model for the history of cosmic star formation, Mon. Not. R. Astron. Soc. **341**, 1253 (2003).
[46] P. S. Behroozi, R. H. Wechsler, and C. Conroy, The average star formation histories of galaxies in dark matter halos from $z = 0$–8, Astrophys. J. **770**, 57 (2013).
[47] P. Madau and M. Dickinson, Cosmic star-formation history, Annu. Rev. Astron. Astrophys. **52**, 415 (2014).
[48] N. Aghanim *et al.* (Planck Collaboration), Planck 2018 results. VI. Cosmological parameters, Astron. Astrophys. **641**, A6 (2020).
[49] C. W. Misner, K. S. Thorne, and J. A. Wheeler, *Gravitation* (W. H. Freeman and Company, San Francisco, 2017).
[50] E. Müller, H. T. Janka, and A. Wongwathanarat, Parametrized 3D models of neutrino-driven supernova explosions. Neutrino emission asymmetries and gravitational-wave signals, Astron. Astrophys. **537**, A63 (2012).
[51] H. Andresen, The study of gravitational waves from three-dimensional simulations of core-collapse supernovae, Ph.D. thesis, (Technische Universität, Munich, 2017).
[52] K. N. Yakunin, A. Mezzacappa, P. Marronetti, S. Yoshida, S. W. Bruenn, W. R. Hix, E. J. Lentz, O. E. Bronson Messer, J. A. Harris, E. Endeve, J. M. Blondin, and E. J. Lingerfelt, Gravitational wave signatures of *ab initio* two-dimensional core collapse supernova explosion models for 12–25 $M_\odot$ stars, Phys. Rev. D **92**, 084040 (2015).
[53] H. Andresen, E. Müller, and H. T. Janka, Gravitational waves from three-dimensional core collapse supernova simulations, in *50th Rencontres de Moriond on Gravitation: 100 years after GR* (Rencontres de Moriond, La Thuile, 2015).
[54] T. Kuroda, K. Kotake, and T. Takiwaki, A new gravitational-wave signature from standing accretion shock instability in supernovae, Astrophys. J. Lett. **829**, L14 (2016).
[55] E. P. OConnor and S. M. Couch, Exploring fundamentally three-dimensional phenomena in high-fidelity simulations of core-collapse supernovae, Astrophys. J. (Online) **865** (2018).
[56] H. Andresen, E. Mller, H.-T. Janka, A. Summa, K. Gill, and M. Zanolin, Gravitational waves from 3D core-collapse supernova models: The impact of moderate progenitor rotation, Mon. Not. R. Astron. Soc. **486**, 2238 (2019).
[57] J. Powell and B. Müller, Gravitational wave emission from 3D explosion models of core-collapse supernovae with low and normal explosion energies, Mon. Not. R. Astron. Soc. **487**, 1178 (2019).
[58] D. Radice, V. Morozova, A. Burrows, D. Vartanyan, and H. Nagakura, Characterizing the gravitational wave signal from

core-collapse supernovae, Astrophys. J. Lett. **876**, L9 (2019).
[59] D. Vartanyan, A. Burrows, and D. Radice, Temporal and angular variations of 3D core-collapse supernova emissions and their physical correlations, Mon. Not. R. Astron. Soc. **489**, 2227 (2019).
[60] J. Powell and B. Mller, Three-dimensional core-collapse supernova simulations of massive and rotating progenitors, Mon. Not. R. Astron. Soc. **494**, 4665 (2020).
[61] A. Mezzacappa, P. Marronetti, R. E. Landfield, E. J. Lentz, K. N. Yakunin, S. W. Bruenn, W. R. Hix, O. E. B. Messer, E. Endeve, J. M. Blondin, and J. A. Harris, Gravitational-wave signal of a core-collapse supernova explosion of a 15 $M_\odot$ star, Phys. Rev. D **102**, 023027 (2020).
[62] H. Andresen, R. Glas, and H. T. Janka, Gravitational-wave signals from 3D supernova simulations with different neutrino-transport methods, Mon. Not. R. Astron. Soc. **503**, 3552 (2021).
[63] J. Powell, B. Mller, and A. Heger, The final core collapse of pulsational pair instability supernovae, Mon. Not. R. Astron. Soc. **503**, 2108 (2021).
[64] S. Shibagaki, T. Kuroda, K. Kotake, and T. Takiwaki, Characteristic time variability of gravitational-wave and neutrino signals from three-dimensional simulations of nonrotating and rapidly rotating stellar core collapse, Mon. Not. R. Astron. Soc. **502**, 3066 (2021).
[65] A. W. Steiner, M. Hempel, and T. Fischer, Core-collapse supernova equations of state based on neutron star observations, Astrophys. J. **774**, 17 (2013).
[66] J. M. Lattimer and F. Douglas Swesty, A generalized equation of state for hot, dense matter, Nucl. Phys. **A535**, 331 (1991).
[67] B. Müller and H. T. Janka, Non-radial instabilities and progenitor asphericities in core-collapse supernovae, Mon. Not. R. Astron. Soc. **448**, 2141 (2015).
[68] M. A. Skinner, J. C. Dolence, A. Burrows, D. Radice, and D. Vartanyan, FORNAX: A flexible code for multiphysics astrophysical simulations, Astrophys. J. Suppl. Ser. **241**, 7 (2019).
[69] O. Just, M. Obergaulinger, and H. T. Janka, A new multidimensional, energy-dependent two-moment transport code for neutrino-hydrodynamics, Mon. Not. R. Astron. Soc. **453**, 3386 (2015).
[70] M. Rampp and H. T. Janka, Radiation hydrodynamics with neutrinos. Variable Eddington factor method for core-collapse supernova simulations, Astron. Astrophys. **396**, 361 (2002).
[71] T. A. Weaver, G. B. Zimmerman, and S. E. Woosley, Presupernova evolution of massive stars, Astrophys. J. **225**, 1021 (1978).
[72] T. Kuroda, T. Takiwaki, and K. Kotake, A new multi-energy neutrino radiation-hydrodynamics code in full general relativity and its application to the gravitational collapse of massive stars, Astrophys. J. Suppl. Ser. **222**, 20 (2016).
[73] H.-T. Janka, Explosion mechanisms of core-collapse supernovae, Annu. Rev. Nucl. Part. Sci. **62**, 407 (2012).
[74] M. A. Pajkos, M. L. Warren, S. M. Couch, E. P. O'Connor, and K.-C. Pan, Determining the structure of rotating massive stellar cores with gravitational waves, Astrophys. J. **914**, 80 (2021).
[75] M. L. Warren, S. M. Couch, E. P. O'Connor, and V. Morozova, Constraining properties of the next nearby core-collapse supernova with multimessenger signals, Astrophys. J. **898**, 139 (2020).
[76] A. Torres-Forné, P. Cerdá-Durán, M. Obergaulinger, B. Müller, and J. A. Font, Universal Relations for Gravitational-Wave Asteroseismology of Protoneutron Stars, Phys. Rev. Lett. **123**, 051102 (2019).
[77] E. Thrane and J. D. Romano, Sensitivity curves for searches for gravitational-wave backgrounds, Phys. Rev. D **88**, 124032 (2013).
[78] R. Jardine, J. Powell, and B. Müller, Gravitational wave signals from two-dimensional core-collapse supernova models with rotation and magnetic fields, Mon. Not. R. Astron. Soc. **510**, 5535 (2022).
[79] R. Raynaud, P. Cerdá-Durán, and J. Guilet, Gravitational wave signature of proto-neutron star convection: I. MHD numerical simulations, Mon. Not. R. Astron. Soc. **509**, 3410 (2021).
[80] R. Epstein, The generation of gravitational radiation by escaping supernova neutrinos, Astrophys. J. **223**, 1037 (1978).
[81] E. Mueller and H. T. Janka, Gravitational radiation from convective instabilities in Type II supernova explosions, Astron. Astrophys. **317**, 140 (1997).
[82] K. Kotake, W. Iwakami, N. Ohnishi, and S. Yamada, Stochastic nature of gravitational waves from supernova explosions with standing accretion shock instability, Astrophys. J. Lett. **697**, L133 (2009).
[83] D. Vartanyan and A. Burrows, Gravitational waves from neutrino emission asymmetries in core-collapse supernovae, Astrophys. J. **901**, 108 (2020).
[84] C. Richardson, M. Zanolin, H. Andresen, M. J. Szczepańczyk, K. Gill, and A. Wongwathanarat, Modeling core-collapse supernovae gravitational-wave memory in laser interferometric data, arXiv:2109.01582.
[85] M. Mukhopadhyay, C. Cardona, and C. Lunardini, The neutrino gravitational memory from a core collapse supernova: Phenomenology and physics potential, J. Cosmol. Astropart. Phys. 07 (2021) 055.
[86] B. Müller and V. Varma, A 3D simulation of a neutrino-driven supernova explosion aided by convection and magnetic fields, Mon. Not. R. Astron. Soc. **498**, L109 (2020).
[87] S. Wang, T. Terada, and K. Kohri, Prospective constraints on the primordial black hole abundance from the stochastic gravitational-wave backgrounds produced by coalescing events and curvature perturbations, Phys. Rev. D **99**, 103531 (2019).
[88] S. Mukherjee, M. S. P. Meinema, and J. Silk, Prospects of discovering sub-solar primordial black holes using the stochastic gravitational wave background from third-generation detectors, Mon. Not. R. Astron. Soc. **510**, 6218 (2022).
[89] N. Bartolo, C. Caprini, V. Domcke, D. G. Figueroa, J. Garcia-Bellido, M. Chiara Guzzetti, M. Liguori, S. Matarrese, M. Peloso, A. Petiteau, A. Ricciardone, M. Sakellariadou, L. Sorbo, and G. Tasinato, Science with the space-based interferometer LISA. IV: probing inflation with gravitational waves, J. Cosmol. Astropart. Phys. 12 (2016) 026.